

Tunnel magnetoresistance of quantum dots coupled to ferromagnetic leads in the sequential and cotunneling regimes

Ireneusz Weymann,^{1,2} Jürgen König,³ Jan Martinek,^{2,4,5} Józef Barnaś,^{1,4} and Gerd Schön²

¹*Department of Physics, Adam Mickiewicz University, 61-614 Poznań, Poland*

²*Institut für Theoretische Festkörperphysik, Universität Karlsruhe, 76128 Karlsruhe, Germany*

³*Institut für Theoretische Physik III, Ruhr-Universität Bochum, 44780 Bochum, Germany*

⁴*Institute of Molecular Physics, Polish Academy of Sciences, 60-179 Poznań, Poland*

⁵*Institute for Materials Research, Tohoku University, Sendai 980-8577, Japan*

(Dated: May 1, 2019)

We study electronic transport through quantum dots weakly coupled to ferromagnetic leads with collinear magnetization directions. Tunneling contributions of first and second order in the tunnel-coupling strength are taken into account. We analyze the tunnel magnetoresistance (TMR) for all combinations of linear and nonlinear response, at or off resonance, with an even or odd dot-electron number. Different mechanisms for transport and spin accumulation the various regimes give rise to different TMR behavior.

PACS numbers: 72.25.Mk, 73.63.Kv, 85.75.-d, 73.23.Hk

I. INTRODUCTION

The study of spin-polarized electron transport through nanostructures with strong Coulomb interaction is a relatively new field of theoretical and experimental research, residing in the intersection of the fields of spintronics [1, 2, 3, 4] and transport through nanostructures [5, 6, 7], respectively. The interplay of finite spin polarization and Coulomb blockade gives rise to a complex transport behavior in which both the electrons' charge and spin degree of freedom play a role [8]. A convenient minimal model system to study this interplay consists of a single-level quantum dot coupled through tunnel barriers to ferromagnetic electrodes. Experimentally such systems may be realized in various ways, including self-assembled dots in ferromagnetic semiconductors [9], ultrasmall aluminum nanoparticles [10], carbon nanotubes [11, 12, 13], or single molecules [14].

The properties of spin-polarized transport through single magnetic tunnel junctions have already proven technological relevance in information-storage devices based on the tunnel magnetoresistance (TMR) effect, i.e., the observation that the current flowing through the junction depends on the relative orientation of the leads' magnetizations. It is maximal for the parallel and minimal for the antiparallel configuration. Quantitatively, it can be characterized by

$$\text{TMR} = \frac{I_P - I_{AP}}{I_{AP}} \quad (1)$$

where I_P and I_{AP} are the currents for the parallel and antiparallel configuration, respectively. Julliere found [15] that the TMR for a single tunnel junction is related to the degree p of spin polarization of the leads' density of states, $p = (\rho^+ - \rho^-)/(\rho^+ + \rho^-)$, by $\text{TMR}^{\text{Jull}} = 2p^2/(1-p^2)$, where ρ^+ and ρ^- are the spin-majority and spin-minority densities of states in the electrodes, respectively. Julliere's formula immediately follows from the fact that the transmission probability of an electron with

spin σ through the barrier is proportional to the product of the (spin-dependent) densities of states for spin σ in source and drain.

Once a nanoscopic island is placed in between the ferromagnetic leads the situation becomes much more complex for two reasons. First, there are different types of transport processes that depend on the leads' spin polarization in a different manner, such as sequential tunneling, non-spin-flip, and spin-flip cotunneling (for non-spin-flip cotunneling an electron of given spin is transferred through the system, while for spin-flip cotunneling both the spin of the transferred electron as well as the dot spin changes during the process). Second, a non-equilibrium spin accumulation can partially polarize the island, which, in turn, affects the total transmission through the device. Therefore, the TMR will, in general, deviate from Julliere's value. It will, furthermore, be different for different transport regimes. The measurement of the TMR as a function of temperature, bias and gate voltages, will, thus, reveal information about the underlying transport processes as well as the spin accumulation on the island.

Spin-dependent transport through a single-level quantum dot in the sequential-tunneling regime with collinearly magnetized leads has been analyzed in Refs. 16, 17, 18. This has been extended [19, 20, 21, 22] to noncollinear configurations with arbitrary relative angle, for which a precession of the dot spin about an intrinsic exchange field gives rise to non-trivial dependence of the angle-dependent conductance. In the present paper, we analyze the TMR for collinear magnetization beyond sequential tunneling. This covers the Coulomb-blockade regime, in which sequential tunneling is exponentially suppressed, and transport is dominated by cotunneling [23, 24, 25, 26, 27, 28, 29]. But even when sequential tunneling is possible, second-order corrections to the current become important for increasing tunnel-coupling strengths. This includes the above-mentioned cotunneling processes but also terms associated with renormaliza-

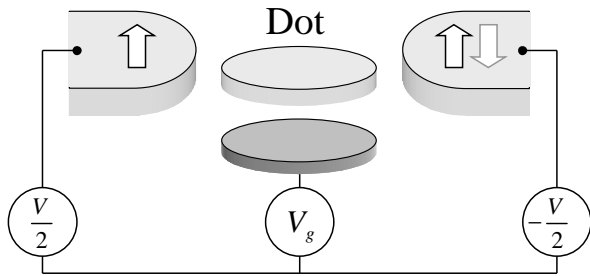


FIG. 1: Single-level quantum dot coupled to ferromagnetic leads. The magnetic moments of the electrodes are either parallel or antiparallel to each other.

tion of level position and tunnel-coupling strength [30]. Recently, we studied spin-dependent transport for a specific transport regime, namely, cotunneling deep inside the Coulomb-blockade valley [31].

Our objective for the present paper is to analyze the TMR in the full parameter space defined by the gate and bias voltages. This includes the linear- and nonlinear-response regime as well as the cases of even and odd dot occupation. We find that the TMR reaches Julliere's value only when the transport is fully carried by non-spin-flip cotunneling. This happens in the Coulomb-blockade valleys in which the dot is either empty or doubly occupied, where the dot remains unpolarized, as well as for large bias voltage in the Coulomb-blockade valley with an odd dot-electron number. For all other regimes, though, the TMR is reduced below Julliere's value.

II. MODEL

We consider transport through a single-level quantum dot. The dot is coupled to two ferromagnetic electrodes with collinear, i.e., either parallel or antiparallel, magnetizations, see Fig. 1. The dot level ε can be tuned by a gate voltage, but is independent of the symmetrically-applied transport voltage.

We model the system by an Anderson-like Hamiltonian of the form

$$H = H_L + H_R + H_D + H_T. \quad (2)$$

The first and second terms represent the left and right reservoirs of noninteracting electrons, $H_r = \sum_{q\sigma} \varepsilon_{rq\sigma} c_{rq\sigma}^\dagger c_{rq\sigma}$, for $r = L, R$, where $c_{rq\sigma}^\dagger$ ($c_{rq\sigma}$) is the creation (annihilation) operator of an electron with wave number q and spin σ in the lead r , whereas $\varepsilon_{rq\sigma}$ denotes the corresponding single-particle energy. The dot is represented by

$$H_D = \sum_{\sigma=\uparrow,\downarrow} \varepsilon d_\sigma^\dagger d_\sigma + U d_\uparrow^\dagger d_\uparrow d_\downarrow^\dagger d_\downarrow, \quad (3)$$

with d_σ^\dagger (d_σ) creating (annihilating) an electron on the dot with spin σ and energy ε , and U is the charging

energy for double occupancy. There are four possible states for the quantum dot: empty dot ($\chi = 0$), singly-occupied dot with a spin-up ($\chi = \uparrow$) or spin-down ($\chi = \downarrow$) electron, and doubly-occupied dot ($\chi = d$). Tunneling between dot and leads is described by

$$H_T = \sum_{r=L,R} \sum_{q\sigma} (t_{rq\sigma} c_{rq\sigma}^\dagger d_\sigma + t_{rq\sigma}^* d_\sigma^\dagger c_{rq\sigma}), \quad (4)$$

where $t_{rq\sigma}$ are the tunnel matrix elements. Tunneling gives rise to an intrinsic broadening Γ^σ of the dot levels, given by the Fermi-golden-rule expression $\Gamma^\sigma = \sum_{r=L,R} \Gamma_r^\sigma$, with $\Gamma_r^\sigma = 2\pi \sum_q |t_{rq\sigma}|^2 \delta(\omega - \varepsilon_{rq\sigma})$. Assuming the matrix elements $t_{rq\sigma}$ to be independent of the wave number and spin orientation, we get $\Gamma_r^\sigma = 2\pi |t_r|^2 \rho_r^\sigma$, with ρ_r^σ denoting the spin-dependent density of states in lead r . In the following we assume the latter to be independent of energy within the electron band. Furthermore, we introduce the degree of spin polarization $p_r = (\rho_r^+ - \rho_r^-)/(\rho_r^+ + \rho_r^-)$ of lead r , and express the four respective couplings in terms of spin polarization as $\Gamma_r^{+(-)} = \Gamma_r(1 \pm p_r)$, where $\Gamma_r = (\Gamma_r^+ + \Gamma_r^-)/2$. In general, the leads may have different spin polarizations and/or coupling strengths to the dot. In the following, however, we assume $p_L = p_R \equiv p$ and $\Gamma_L = \Gamma_R \equiv \Gamma/2$. In the weak coupling regime, typical values of the dot-lead coupling strength Γ are of the order of tens of μeV [27].

III. METHOD AND TRANSPORT EQUATIONS

We calculate the transport properties of the system by making use of a real-time diagrammatic technique [30, 32, 33]. Its main idea is to integrate out the electronic degrees of freedom in the leads in order to arrive at an effective description of the dot subsystem. The dynamics of the subsystem is then described by a reduced, four-dimensional, density matrix with density matrix elements $P_{\chi_2}^{\chi_1}(t)$. The time evolution of the reduced system can be represented graphically as a sequence of irreducible diagrams on the Keldysh contour. An example of such time evolution is shown in Fig. 2, where the upper and lower branches of the Keldysh contour represent the forward

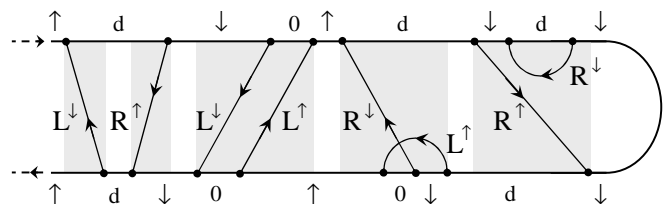


FIG. 2: An example for the time evolution of the reduced density matrix. The grey regions define irreducible diagrams of first and second order in tunneling, respectively. The direction of each tunneling line indicates whether an electron of respective spin leaves or enters the dot, thus, leading to a change of the dot state, as indicated on the forward and backward Keldysh propagators.

and backward propagators. Tunneling is represented by vertices, that are connected in pairs by tunnel lines. Each grey region in Fig. 2 defines an irreducible diagram that corresponds to a transition of the dot state. First- and second-order transport in the tunnel-coupling strength Γ is described by diagrams containing one or two tunnel lines, respectively. Since we consider only collinear magnetic configurations of the leads and tunneling is spin conserving, the natural choice of the spin-quantization axis results in vanishing of all non-diagonal density matrix elements, and only the diagonal ones, $P_\chi^x \equiv P_\chi$, need to be considered. They are nothing but the probability to find the dot in state χ .

The time evolution of the reduced density matrix is governed by a generalized master equation [30] that in the stationary limit reduces to

$$0 = \sum_{\chi} \Sigma_{\chi'\chi} P_{\chi}, \quad (5)$$

where $\Sigma_{\chi'\chi}$ describes the irreducible diagram parts with transitions from state χ to χ' . The electric current is given by

$$I = -\frac{ie}{2\hbar} \sum_{\chi\chi'} \Sigma_{\chi'\chi}^I P_{\chi}, \quad (6)$$

where the self energy $\Sigma_{\chi'\chi}^I$ is modified as compared to $\Sigma_{\chi'\chi}$ to account for the number of electrons transferred through the barriers. The rules to calculate $\Sigma_{\chi'\chi}$ and $\Sigma_{\chi'\chi}^I$ are given in the appendix.

Our goal is to calculate the current up to second order in the tunnel-coupling strength Γ . For this, we first expand the self-energies $\Sigma_{\chi'\chi}$ and $\Sigma_{\chi'\chi}^I$ order by order,

$$\Sigma_{\chi'\chi} = \Sigma_{\chi'\chi}^{(1)} + \Sigma_{\chi'\chi}^{(2)} + \dots, \quad (7)$$

where the order corresponds to the number of tunnel lines of a diagram. Consequently, the entire problem is reduced to the calculation of all the self-energies with the aid of the diagrammatic rules.

For an accurate perturbation expansion of the current, we also need to expand the probabilities in orders of Γ ,

$$P_{\chi} = P_{\chi}^{(0)} + P_{\chi}^{(1)} + \dots, \quad (8)$$

with the normalization condition

$$\sum_{\chi} P_{\chi}^{(m)} = \delta_{m,0}. \quad (9)$$

The first- and second-order contributions to the current are then given by

$$I^{(1)} = -\frac{ie}{2\hbar} \sum_{\chi\chi'} \Sigma_{\chi'\chi}^{I(1)} P_{\chi}^{(0)} \quad (10)$$

$$I^{(2)} = -\frac{ie}{2\hbar} \sum_{\chi\chi'} \left[\Sigma_{\chi'\chi}^{I(2)} P_{\chi}^{(0)} + \Sigma_{\chi'\chi}^{I(1)} P_{\chi}^{(1)} \right]. \quad (11)$$

To determine $P_{\chi}^{(0)}$ and $P_{\chi}^{(1)}$, we have to expand the master equation, Eq. (5), order by order,

$$0 = \sum_{\chi} \Sigma_{\chi'\chi}^{(1)} P_{\chi}^{(0)} \quad (12)$$

$$0 = \sum_{\chi} \Sigma_{\chi'\chi}^{(2)} P_{\chi}^{(0)} + \Sigma_{\chi'\chi}^{(1)} P_{\chi}^{(1)}. \quad (13)$$

The evaluation of $P_{\chi}^{(0)}$ and $P_{\chi}^{(1)}$ from Eqs. (12) and (13) has to be done with some care. As we will see below, we have to distinguish between the two cases in which sequential tunneling is either present or exponentially suppressed.

A. Perturbation expansion in the presence of sequential tunneling

In regime where the sequential tunneling is allowed, one can use the perturbation expansion presented in the previous subsection. In particular, one can determine the zeroth-order probabilities $P_{\chi}^{(0)}$ from Eq. (12) and, then, plug the result into Eq. (13) in order to evaluate the first-order corrections $P_{\chi}^{(1)}$. Having calculated the probabilities, one can use the result to get the current from Eqs. (10) and (11) in first and second order, respectively.

B. Perturbation expansion in the Coulomb-blockade regime

In the Coulomb-blockade regime, several of the first-order self-energies are exponentially small as they are associated with energetically forbidden sequential-tunneling rates. As a consequence, all addends in the first-order master equation, Eq. (12), are exponentially small: either the state χ is classically forbidden, i.e., $P_{\chi}^{(0)}$ is exponentially suppressed, or the state χ is classically allowed but then the corresponding self energies $\Sigma_{\chi'\chi}^{(1)}$ are exponentially small.

This is not a problem for the Coulomb-blockade valleys with an even number of electrons, $k_B T, |eV| \ll \varepsilon, \varepsilon + U$ and $k_B T, |eV| \ll -\varepsilon, -\varepsilon - U$, since for this case, the first-order master equation, Eq. (12), yields $P_{\chi}^{(0)} = \delta_{\chi,0}$ and $P_{\chi}^{(0)} = \delta_{\chi,d}$, respectively, i.e., there is only one classically-allowed dot state. The situation is different for the Coulomb-blockade valley with an odd number of electrons, $k_B T, |eV| \ll -\varepsilon, \varepsilon + U$, where both $\chi = \uparrow$ and $\chi = \downarrow$ are classically occupied. In this case, Eq. (12) simplifies to

$$\begin{pmatrix} \Sigma_{00}^{(1)} & 0 & 0 & 0 \\ \Sigma_{\uparrow 0}^{(1)} & 0 & 0 & \Sigma_{\uparrow d}^{(1)} \\ \Sigma_{\downarrow 0}^{(1)} & 0 & 0 & \Sigma_{\downarrow d}^{(1)} \\ 0 & 0 & 0 & \Sigma_{dd}^{(1)} \end{pmatrix} \begin{pmatrix} P_0^{(0)} \\ P_{\uparrow}^{(0)} \\ P_{\downarrow}^{(0)} \\ P_d^{(0)} \end{pmatrix} = 0, \quad (14)$$

i.e., we obtain $P_0^{(0)} = P_d^{(0)} = 0$ while the individual occupations $P_\uparrow^{(0)}$ and $P_\downarrow^{(0)}$ remain undetermined. Furthermore, we find that $P_\uparrow^{(1)}$ and $P_\downarrow^{(1)}$ drop out of the second-order master equation, Eq. (13), and the expression for the second-order current, Eq. (11), since they are multiplied with exponentially small transition rates $\Sigma_{\chi'\chi}^{(1)}$. As a consequence, all the needed probabilities $P_0^{(1)}$, $P_\uparrow^{(0)}$, $P_\downarrow^{(0)}$, and $P_d^{(1)}$ are determined from Eq. (13) alone, which simplifies to

$$\begin{pmatrix} \Sigma_{00}^{(1)} & \Sigma_{0\uparrow}^{(2)} & \Sigma_{0\downarrow}^{(2)} & 0 \\ \Sigma_{\uparrow 0}^{(1)} & \Sigma_{\uparrow\uparrow}^{(2)} & \Sigma_{\uparrow\downarrow}^{(2)} & \Sigma_{\uparrow d}^{(1)} \\ \Sigma_{\downarrow 0}^{(1)} & \Sigma_{\downarrow\uparrow}^{(2)} & \Sigma_{\downarrow\downarrow}^{(2)} & \Sigma_{\downarrow d}^{(1)} \\ 0 & \Sigma_{d\uparrow}^{(2)} & \Sigma_{d\downarrow}^{(2)} & \Sigma_{dd}^{(1)} \end{pmatrix} \begin{pmatrix} P_0^{(1)} \\ P_\uparrow^{(0)} \\ P_\downarrow^{(0)} \\ P_d^{(1)} \end{pmatrix} = 0, \quad (15)$$

plus $P_\uparrow^{(0)} + P_\downarrow^{(0)} = 1$ from the normalization condition.

If one were ignorant about the described subtlety one might naively use the first-order master equation, Eq. (12), with all its exponentially small (but finite) addends to obtain a well-defined (but, in general, wrong) result for $P_\uparrow^{(0)}$ and $P_\downarrow^{(0)}$. There are situations, though, in which this procedure, although unjustified by construction, leads to the correct result, namely when the total system is symmetric under spin reversal (nonmagnetic leads, $p = 0$), or for vanishing bias voltage, $V = 0$. In both cases, the correct result $P_\uparrow^{(0)} = P_\downarrow^{(0)} = 1/2$ is ensured either by symmetry or as a consequence of detailed balance relations. It is only for broken spin symmetry combined with finite bias voltage $V \neq 0$ that the naive procedure leads to wrong results.

We remark that the current in the Coulomb-blockade regime far from resonance can alternatively be calculated without the use of the diagrammatic language. Instead one can employ a rate-equation approach with cotunneling rates obtained in second-order perturbation theory [23, 24, 25]. The rate $\gamma_{r'r}^{\sigma'\leftarrow\sigma}$ for a cotunneling process, in which one electron leaves the dot to reservoir r' and one electron enters from r with the initial and final dot state being σ and σ' , respectively, is

$$\gamma_{r'r}^{\sigma'\leftarrow\sigma} = \frac{1}{2\pi} \text{Re} \int d\omega [1 - f(\omega - \mu_r)] f(\omega - \mu_{r'}) \times \left[\frac{\Gamma_r^\sigma \Gamma_{r'}^\sigma}{(\omega - \varepsilon + i0^+)^2} + \frac{\Gamma_r^{\bar{\sigma}} \Gamma_{r'}^{\bar{\sigma}}}{(\omega - \varepsilon - U + i0^+)^2} \right] \quad (16)$$

when the dot spin is not changed ($\sigma = \sigma'$) – *non-spin-flip cotunneling*, while we get

$$\gamma_{r'r}^{\bar{\sigma}\leftarrow\sigma} = \frac{\Gamma_r^\sigma \Gamma_{r'}^{\bar{\sigma}}}{2\pi} \text{Re} \int d\omega [1 - f(\omega - \mu_r)] f(\omega - \mu_{r'}) \times \left(\frac{1}{\omega - \varepsilon + i0^+} + \frac{1}{\varepsilon + U - \omega + i0^+} \right)^2, \quad (17)$$

for cotunneling process in which the dot spin is flipped ($\bar{\sigma}$ is the opposite spin of σ) – *spin-flip cotunneling*. Here,

$f(\omega - \mu_r)$ is the Fermi function of reservoir r with electrochemical potential μ_r . The regularization $+i0^+$ is put here by hand, while it naturally comes out within the diagrammatic formulation. There are two types of spin-flip cotunneling processes. Each of them involves two tunneling events, either through the same or through the two opposite tunnel barriers. Accordingly, we refer to them as *single-barrier* ($r = r'$) and *double-barrier cotunneling* ($r \neq r'$). Double-barrier cotunneling contributes directly to the current, while single-barrier cotunneling preserves the total charge in the leads. Nevertheless, spin-flip single-barrier cotunneling can influence the total current indirectly, by changing of the magnetic state of the dot. The probabilities P_σ are obtained from the stationary rate equation $0 = \sum_{rr'} [\gamma_{r'r}^{\downarrow\leftarrow\uparrow} P_\uparrow - \gamma_{r'r}^{\uparrow\leftarrow\downarrow} P_\downarrow]$ together with the normalization condition $P_\uparrow + P_\downarrow = 1$. The current I is, then, given by

$$I = \frac{e}{\hbar} \sum_{\sigma\sigma'} [\gamma_{RL}^{\sigma'\leftarrow\sigma} - \gamma_{LR}^{\sigma'\leftarrow\sigma}] P_\sigma. \quad (18)$$

This result is identical to the one obtained within the diagrammatic technique. Close to resonance, however, it is not sufficient to include the sequential and cotunneling processes, but also contributions associated with renormalization of level position, level splitting and tunnel-coupling strengths become important. The diagrammatic language systematically takes everything into account properly.

C. Crossover scheme

For both the case when sequential tunneling is allowed or suppressed, we have formulated a proper perturbation expansion of the current up to second order in the tunnel-coupling strength. When evaluating the TMR as a function of various parameters, such as the gate or transport voltage, one has to switch from one scheme to the other around the threshold of sequential tunneling. At the crossover, there is no well-defined second-order perturbation expansion since terms of different order in Γ are comparable in magnitude, and their ratio changes continuously as a function of gate or transport voltage. Alternatively, we may use a crossover scheme that smoothly crosses over from one scheme to the other. This scheme consists of solving the master equation with first- and second-order self energies, without expanding the probabilities,

$$0 = \sum_x [\Sigma_{\chi'\chi}^{(1)} + \Sigma_{\chi'\chi}^{(2)}] P_\chi, \quad (19)$$

and plugging this into the expression for the current,

$$I = -\frac{ie}{2\hbar} \sum_{xx'} [\Sigma_{\chi'\chi}^{I(1)} + \Sigma_{\chi'\chi}^{I(2)}] P_\chi. \quad (20)$$

Up to second order in Γ , this result for the current is identical to the above-introduced accurate perturbation

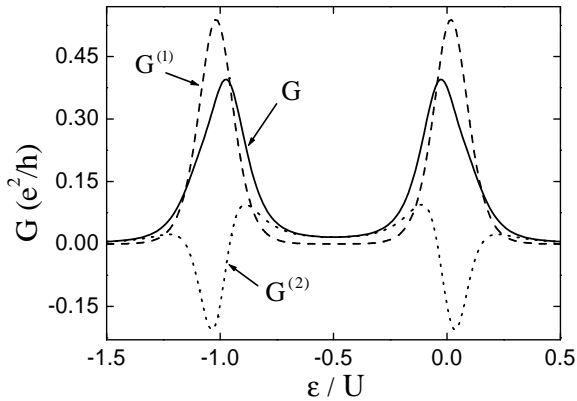


FIG. 3: Linear conductance for nonmagnetic leads ($p = 0$) as a function of the level position. The dashed line corresponds to the first-order contribution $G^{(1)}$, the dotted line represents the second-order conductance $G^{(2)}$ and the solid line presents the sum $G^{(1)} + G^{(2)}$. The parameters are: $k_B T = \Gamma$ and $U = 20\Gamma$. The figure was generated using the scheme for the perturbation expansion in the presence of sequential tunneling.

schemes. Deviations are of third and higher order, which are, although unsystematic, always small for the chosen parameters, as otherwise, the perturbation expansion would break down anyway.

IV. RESULTS

A. Nonmagnetic leads

Before presenting the results on the TMR for quantum dots attached to ferromagnetic leads, we illustrate the perturbation scheme introduced above for nonmagnetic leads. In Fig. 3 we show the linear conductance as a function of the level position (that can be tuned by a gate voltage), calculated to first (dashed line) and second (dotted line) order as well as the sum of both contributions (solid line). Resonance peaks appear when either ε or $\varepsilon + U$ crosses the Fermi energy of the leads. Away from resonance sequential tunneling is exponentially suppressed, and cotunneling processes dominate transport. But also at resonance, second-order contributions are important, as can be seen in the figure. In particular, they yield a shift of the peak position and introduce an additional broadening.

B. Ferromagnetic leads

We now switch to the case of ferromagnetic leads. As a consequence of spin-dependent densities of states in the leads, the dot-lead coupling strength becomes spin dependent as well. The coupling of the dot level to the leads acquire a factor $(1 + p)$ or $(1 - p)$ for coupling to majority or minority spins, respectively. We assume that

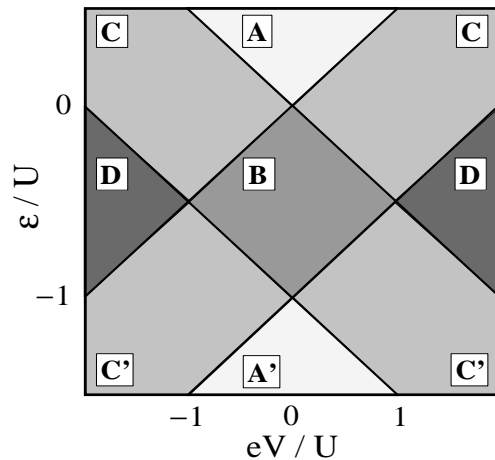


FIG. 4: A sketch presenting different transport regimes. The respective regimes are separated by solid lines.

spin-up (spin-down) electrons in the parallel configuration correspond to the majority (minority) electrons of the leads. In the antiparallel configuration, on the other hand, the magnetic moment of the right electrode is reversed, and spin-up (spin-down) corresponds to minority (majority) electrons in the right lead.

One of the main results of this paper is that the TMR strongly depends on the transport regime. The various transport regimes are sketched in Fig. 4.

In the three diamonds around $V = 0$ the number of dot electrons is fixed (to 0 in regime A, 1 in regime B, and 2 in regime A'), and sequential tunneling is suppressed. Sequential tunneling sets in once the bias voltage is increased above the threshold voltage, allowing for finite occupation of two adjacent charge states (0 and 1 for regime C, and 1 and 2 for regime C'). In regime D all charge states 0,1, and 2 are possible. By performing a particle-hole transformation, the behavior in regime A' and C' can be mapped to that in regime A and C, respectively.

C. Sequential tunneling

For reference, we list the TMR values obtained in first-order perturbation theory (see also Fig. 5). In regimes A (and A'), B, and D, the TMR value is

$$\text{TMR}_{\text{seq}}^{\text{A,B,D}} = \frac{p^2}{1 - p^2} = \frac{1}{2} \text{TMR}^{\text{Jull}}, \quad (21)$$

while for regime C (and C') it is

$$\text{TMR}_{\text{seq}}^{\text{C}} = \frac{4p^2}{3(1 - p^2)} = \frac{2}{3} \text{TMR}^{\text{Jull}}. \quad (22)$$

Within sequential tunneling the TMR through a quantum-dot spin valve is always smaller than Julliere's value for a *single magnetic tunnel junction*. In the latter case, electrons are directly tunneling from one lead to

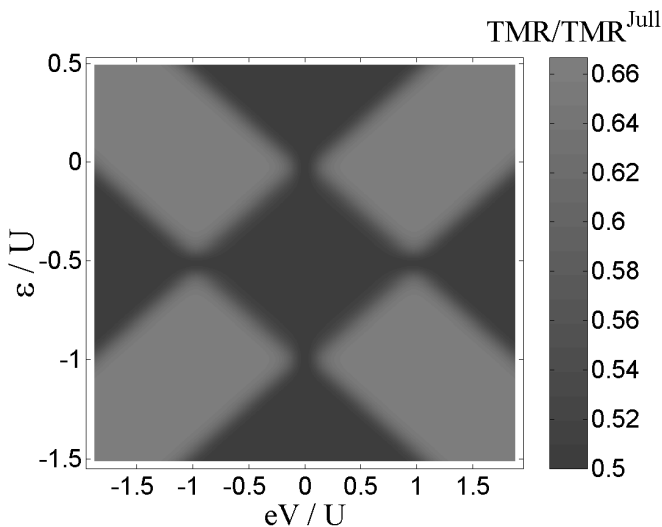


FIG. 5: The first-order tunnel magnetoresistance as a function of the bias and gate voltages. The parameters are: $k_B T = 1.5\Gamma$, $U = 40\Gamma$, and $p = 0.5$.

the other. The transmission is, therefore, proportional to the product of the (spin-dependent) densities of states of both leads, i.e., proportional to $(1+p)^2$ in case the spin of the transferred electron belongs to the majority spins in both leads, $(1-p)^2$ in case it belongs to the minority spins, and $(1+p)(1-p)$ in case it is majority spin in one and minority spin in the other lead. The total current for the parallel and antiparallel configurations is, thus, proportional to $1+p^2$ and $1-p^2$, respectively, which yields Julliere's value for the TMR.

The sequential tunneling rates in a quantum-dot spin valve involve the (spin-dependent) density of states of one lead only and are independent of the orientation of the other lead. To get a finite TMR, one needs to take into account *nonequilibrium spin accumulation* on the quantum dot, which is induced by the spin dependence of the tunneling rates. In the antiparallel configuration, the dot hosts a nonequilibrium spin accumulation $m = (P_\uparrow - P_\downarrow)/2$ due to a different occupation of up- and down-spin levels in the dot, $P_\uparrow \neq P_\downarrow$. It is, thus, the spin accumulation on the dot that mediates the information about the relative magnetic orientation of the leads. This indirect mechanism is, however, always less effective than a direct coupling of the two leads, which is why the sequential-tunneling TMR is always smaller than Julliere's value.

The result $\text{TMR} = \frac{1}{2}\text{TMR}^{\text{Jull}}$ is characteristic of ferromagnet/normal-metal/ferromagnet double tunnel junctions without Coulomb interaction [34], i.e., in the absence of any electron correlations, as well as for quantum dots with vanishing interaction $U \rightarrow 0$. For the regime D all three charge states play a role as for non-interacting case so the value of TMR also corresponds to this situation. The same value is reached in the Coulomb-blockade regimes A (A') and B, because all

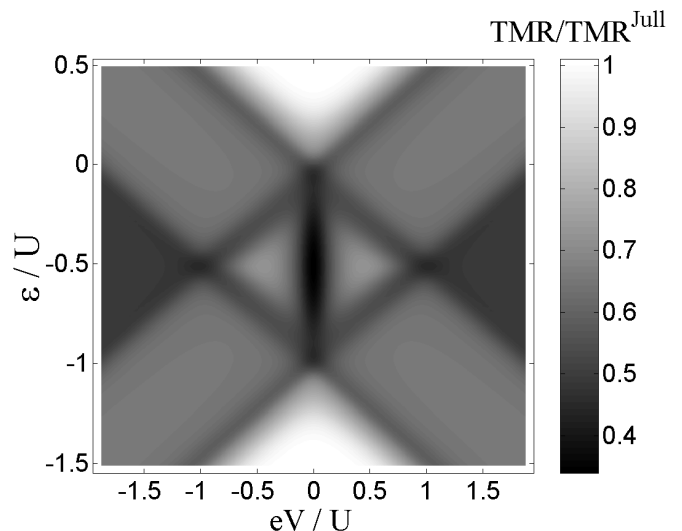


FIG. 6: The first-plus-second-order tunnel magnetoresistance as a function of bias and gate voltage. The parameters are the same as in Fig. 5. The figure was generated using the crossover scheme.

transport processes in this regime are possible only due to hot electrons, which effectively do not feel the Coulomb barrier, interaction, and correlations. In regime C (C') Coulomb interaction is important and gives rise to the result $\text{TMR} = \frac{2}{3}\text{TMR}^{\text{Jull}}$. This increased TMR is related with the presence of a nonequilibrium spin accumulation and induced by it an additional charge accumulation for the antiparallel alignment. To illustrate this let us consider regime C for large bias voltages such that electrons are always entering the dot from the left and are leaving to the right lead. For the parallel alignment the dot occupancy is given by $P_\uparrow = P_\downarrow = P_0 = \frac{1}{3}$ and $P_d = 0$, while the current I does not depend on the spin polarization p . For the antiparallel alignment, the spin-current conservation condition $I_L^\sigma = I_r^\sigma$, with I_r^σ being the current flowing through the barrier r in the spin channel σ , yields $(1+p)P_0 = (1-p)P_\uparrow$ and $(1-p)P_0 = (1+p)P_\downarrow$, i.e., the probability $P_0 = (1-p^2)/(3+p^2)$ to find the dot empty is reduced. Due to the fact that the current $I \sim P_0$ (coming from the left lead) for both alignments, the tunnel magnetoresistance acquires the value $\frac{2}{3}\text{TMR}^{\text{Jull}}$.

As in regimes A and B sequential tunneling is exponentially suppressed, the TMR value obtained in first-order perturbation theory is unreliable. The TMR due to cotunneling will be significantly different, as shown below. In regimes C and D, on the other hand, sequential tunneling is present, and second-order corrections lead to smaller deviations only.

D. Sequential tunneling plus cotunneling

The TMR of first- plus second-order transport is shown in Fig. 6, where the second-order result is obtained by the

crossover scheme. It is clear that second-order transport has the strongest impact on the TMR in the Coulomb-blockade regime (regimes A and B). In regime B we even find a distinctively different behavior for the linear- and the nonlinear-response regimes. For regimes C and D, corrections due to second-order transport are smaller. With our theory we are able to cover all the transport regimes including the crossover region. In the following we analyze the various transport regimes in detail.

1. Regime A

In the Coulomb-blockade regime A the dot is empty, and the TMR is just due to spin-dependent non-spin-flip cotunneling through the dot. There is no spin accumulation on the dot. The cotunneling rates are proportional to the product of the density of states of the left and right leads. In this regime electrons directly tunnel from one lead to the other similar as for a single magnetic tunnel junction case. Thus, the current flowing in the parallel configuration is proportional to $1 + p^2$, whereas that flowing in the antiparallel configuration is proportional to $1 - p^2$. As a consequence, the TMR is that of a single magnetic tunnel junction,

$$\text{TMR}^A = \frac{2p^2}{1 - p^2} = \text{TMR}^{\text{Jull}}, \quad (23)$$

i.e., twice as large as obtained within the sequential-tunneling approximation.

In the regime A' the dot is occupied by two electrons and transport has hole-like character with only non-spin-flip cotunneling as for the regime A, consequently the tunnel magnetoresistance has the same value.

2. Regime B

The TMR in regime B displays several nontrivial features. In particular, it is not constant but depends on both the gate and bias voltage. Furthermore, we find that for nonlinear response the TMR is significantly enhanced as compared to linear response. In contrast, the TMR in the adjacent Coulomb blockade valley with even number of electrons, regime A, is rather trivial. This parity effect is related to the fact that the singly-occupied dot in regime B can be (partially) spin polarized, while the empty or doubly-occupied dot in regime A and A' respectively is nonmagnetic.

The TMR in regime B is substantially smaller than that in regime A. This can be understood by the fact that for a singly-occupied dot both spin-flip and non-spin-flip cotunneling processes are possible, in contrast to regime A and A' where only non-spin-flip cotunneling occurs. There is a perfect symmetry in transmission magnitude between spin-flip (non-spin-flip) processes in the parallel and non-spin-flip (spin-flip) in the antiparallel configuration, so in the absence of spin accumulation

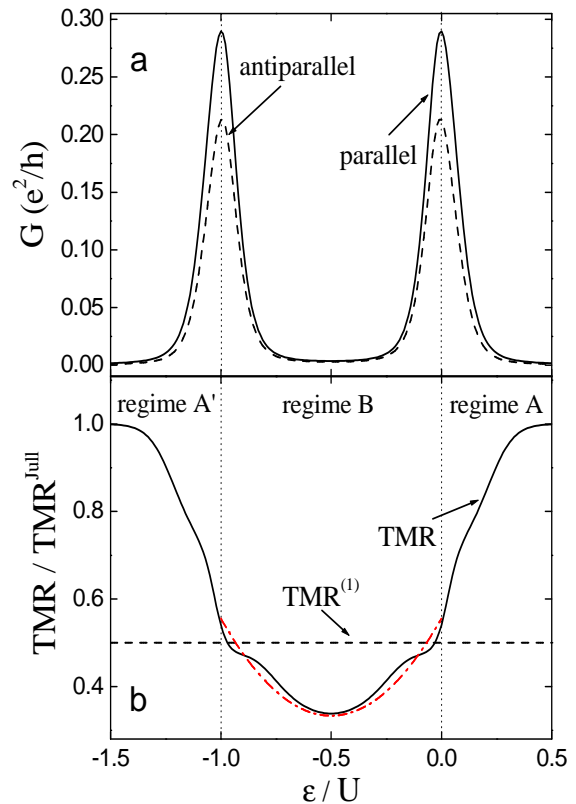


FIG. 7: The total linear conductance (a) in the parallel (solid line) and antiparallel (dashed line) configuration and the resulting tunnel magnetoresistance [solid line in (b)] as a function of the level position. The dashed line in part (b) represents the first-order tunnel magnetoresistance. The dotted-dashed curve presents the TMR calculated using the approximation Eq. (24). The parameters are $k_B T = 1.5\Gamma$, $U = 40\Gamma$, and $p = 0.5$. The figure was generated using the scheme for the perturbation expansion in the presence of sequential tunneling.

($P_\uparrow = P_\downarrow$) the resulting TMR would be reduced to zero. Only due to the presence of spin accumulation ($P_\uparrow \neq P_\downarrow$) for the antiparallel alignment transport is reduced and $\text{TMR} > 0$. Therefore, the actual value of the TMR in regime B depends in a sensitive way on the processes determining the spin accumulation, which is a function of both the gate and bias voltage. In particular, the different role of spin-relaxation channels for the linear- and non-linear-response regime give rise to qualitatively different behavior for the two cases.

We first consider the *linear-response* TMR as a function of level position (or gate voltage), as displayed in Fig. 7. The figure presents the linear conductance in the parallel and antiparallel configurations (part a) and the TMR (part b). We plot the first-order $\text{TMR}^{(1)}$, which is constant and equal to half of the Julliere's value. First of all, one can see that the inclusion of second-order processes modifies the TMR substantially. The total TMR is well below Julliere's value as a consequence of spin-flip cotunneling. It is minimal in the center of the Coulomb-

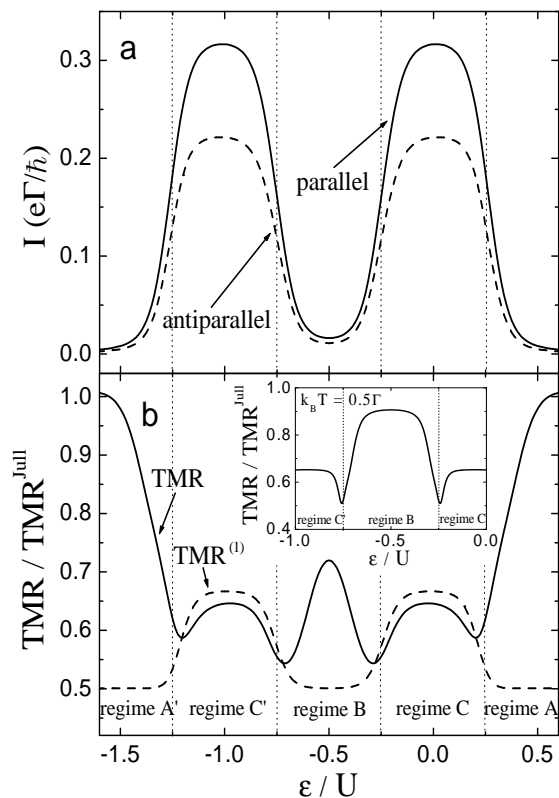


FIG. 8: The total currents (a) in the parallel (solid line) and antiparallel (dashed line) magnetic configurations as a function of level position for $eV = 20\Gamma$. Part (b) shows the first-order contribution to the TMR (dashed line) and the total TMR (solid line). The inset in part (b) shows the total TMR at lower temperature, $k_B T = 0.5\Gamma$. The other parameters are the same as in Fig. 7. The figure was generated using the crossover scheme.

blockade valley, $\varepsilon = -U/2$, where the relative importance of spin-flip as compared to non-spin-flip cotunneling is strongest. To estimate the gate-voltage dependence of this relative importance we consider the ratio of the spin-flip over the non-spin-flip cotunneling rate, as given in Eqs. (17) and (16). Since we are only interested in the gate-voltage dependence we simply take the energy denominators at $\omega = 0$ and find that the ratio scales with $[-1/\varepsilon + 1/(\varepsilon + U)]^2 / [1/\varepsilon^2 + 1/(\varepsilon + U)^2] = 2/[1 + (1 + 2\varepsilon/U)^2]$, which is maximal for $\varepsilon = -U/2$. As illustrated in Fig. 7b, the gate-voltage dependence of the TMR around the center is parabolic. To obtain an approximate analytic expression for the linear-response TMR, we specify our full result for the Coulomb-blockade regime ($k_B T, \Gamma \ll -\varepsilon, \varepsilon + U$), and take into account only the lowest-order corrections in the ratio x/y with $x = |eV|$, $k_B T$, $y = |\varepsilon|, \varepsilon + U$. To describe the parabolic behavior, we, furthermore, expand the TMR up to quadratic order around $\varepsilon = -U/2$ and obtain

$$\text{TMR}^B = \frac{p^2}{1-p^2} \left[\frac{2}{3} + \frac{4}{9} \left(1 + \frac{2\varepsilon}{U} \right)^2 \right]. \quad (24)$$

We find that the smallest TMR value is $1/3$ of that in regime A. As seen in Fig. 7b, this analytic expression approximates the numerical data quite well.

We now switch to the *non-linear-response* regime. This case is illustrated in Fig. 8, where the currents in the parallel and antiparallel configuration as well as the resulting TMR are plotted as a function of the level position for $eV = 20\Gamma$. The dashed line in Fig. 8b presents the first-order TMR plotted for reference. When changing the position of the dot level, one crosses over from regime A' over C' to B, and then further through C to A. It can be seen that the behavior of TMR in regime B differs significantly from that in linear response, Fig. 7b. Instead of a minimum, we find a local maximum for $\varepsilon = -U/2$, as displayed in Fig. 8b. When lowering the temperature, we even find a pronounced plateau of the TMR, with the plateau height given by Julliere's value and the widths determined by the region where first-order contributions are negligible. The reason for this increased TMR is nonequilibrium spin accumulation. The presence of double-barrier spin-flip cotunneling, on the one hand, tends to decrease the TMR as discussed above. At the same time, on the other hand, it gives rise to spin accumulation that increases the TMR. As it turns out, the two effects compensate each other in the nonlinear-response regime ($eV \gg k_B T$), such that the TMR equals Julliere's value as if spin-flip cotunneling were absent. This compensation does not occur in the linear-response regime since in that case single-barrier spin-flip cotunneling processes become important, which do not contribute to transport but reduce the spin accumulation. When approaching the threshold for sequential tunneling, the TMR drops from Julliere's value to match the first-order TMR⁽¹⁾. At higher temperature, such that the plateau is not yet fully developed a local maximum still survives.

The different behavior of the linear- and nonlinear-response regime is also nicely seen in the TMR as a function of transport voltage. The current for the parallel and antiparallel configuration as well as the resulting TMR is shown in Fig. 9 for $\varepsilon = -U/2$. Unlike the first-order TMR⁽¹⁾ illustrated in Fig. 9b by a dashed line, the total TMR is a nonmonotonic function of the bias voltage, which can be understood from the discussions presented in above. For bias voltages below the threshold of sequential tunneling, transport is dominated by cotunneling. Double-barrier spin-flip cotunneling processes suppress the TMR as compared to the Julliere's value. A finite spin accumulation, on the other hand, weakens this suppression and, therefore, tends to increase the TMR. In the linear-response regime, $|eV| \ll k_B T$, the presence of single-barrier spin-flip cotunneling reduces the spin accumulation which results in a rather low TMR. This is no longer the case at large bias, $|eV| \gg k_B T$, where only single-barrier spin-flip cotunneling plays no role and the net effect of double-barrier spin-flip cotunneling on the TMR is compensated. As a result we find an increase of the TMR in regime B with increasing bias voltage within

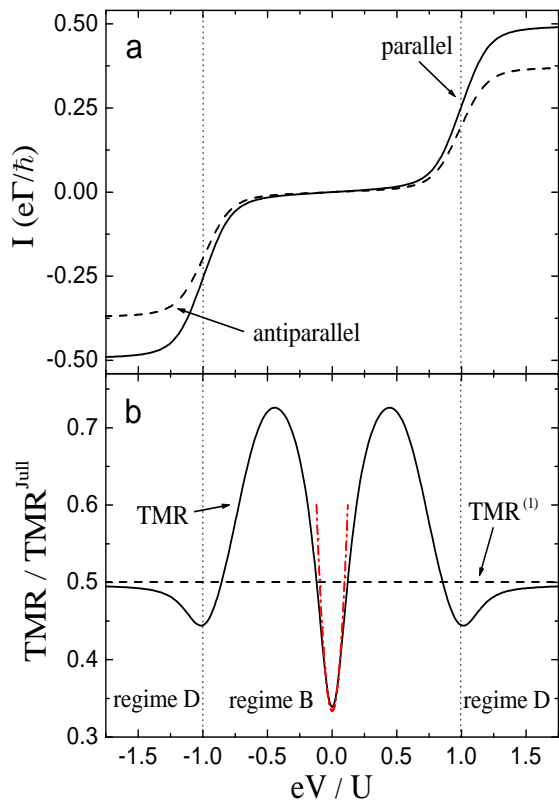


FIG. 9: The total current (a) in the parallel (solid line) and antiparallel (dashed line) magnetic configurations as a function of the bias voltage. Part (b) shows the first-order contribution to the TMR (dashed line) and the total TMR (solid line). The dotted-dashed curve presents the TMR calculated using the approximation Eq. (26). The parameters are: $k_B T = 1.5\Gamma$, $\varepsilon = -U/2$, $U = 40\Gamma$, and $p = 0.5$. The figure was generated using the crossover scheme.

the limits

$$\frac{1}{3}\text{TMR}^{\text{Jull}} \leq \text{TMR}^{\text{B}} \leq \text{TMR}^{\text{Jull}}. \quad (25)$$

The minimal value is reached at $V = 0$ and $\varepsilon = -U/2$, as discussed in the previous paragraph, and the maximal value is approached for bias voltages large as compared to temperature but still far away from the onset of sequential tunneling. For an approximate analytic expression of the TMR around the minimum, we consider the symmetric Anderson model, $\varepsilon = -U/2$, expand the TMR up to quadratic order in $|eV|/k_B T$ and go to the limit $|\varepsilon| \gg k_B T$. The result,

$$\text{TMR}^{\text{B}} = \frac{p^2}{1-p^2} \left[\frac{2}{3} + \frac{(3-p^2)(eV)^2}{54(k_B T)^2} \right], \quad (26)$$

which compares well with the full numerical result, as can be seen in Fig. 9b. When further increasing the bias voltage, sequential tunneling sets in. Deep in the regime D the TMR approaches one half of Julliere's value. As a consequence, the TMR has to decrease in the crossover

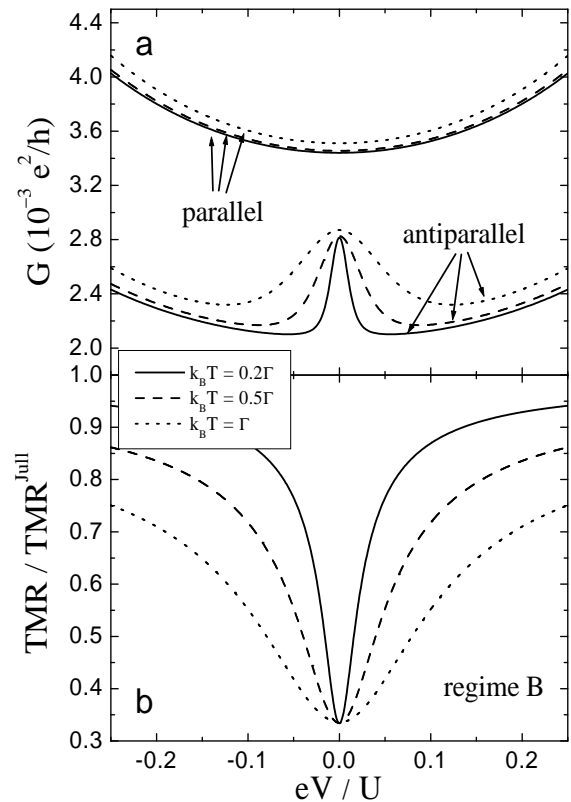


FIG. 10: The differential conductance (a) for parallel and antiparallel configurations and the tunnel magnetoresistance (b) as a function of the bias voltage for different values of temperature. The maximum in conductance for antiparallel configuration at zero bias is clearly demonstrated. The other parameters are the same as in Fig. 9. Figure was generated using the scheme for the perturbation expansion in the Coulomb blockade regime.

regime between regimes B and D to match the correct asymptotic behavior, this is shown in Fig. 9.

There is one more extra feature directly at the threshold voltage for sequential tunneling. At this point, sequential tunneling dominates transport but second-order corrections are still important. As shown in Fig. 9, this correction gives rise to a local minimum of the TMR as function of the bias voltage. To get an approximate analytic expression for the TMR at this intersection point of regimes B, C and D, we assume $|\varepsilon| \gg k_B T$ and expand the TMR up to first order in $\Gamma/(k_B T)$ to get

$$\text{TMR}^{\text{B|C|D}} = \frac{p^2}{1-p^2} \times \left\{ 1 - \frac{\Gamma}{4\pi k_B T} \left[\ln \left(\frac{|\varepsilon|}{\pi k_B T} \right) - \Psi \left(\frac{1}{2} \right) \right] \right\}, \quad (27)$$

with $\Psi(x)$ being the digamma function, $\Psi(1/2) \simeq -1.96$.

The anomalous behavior of the TMR in the Coulomb-blockade regime is generated by the interplay of single- and double-barrier cotunneling for the antiparallel configuration. This is also seen in the appearance of a pro-

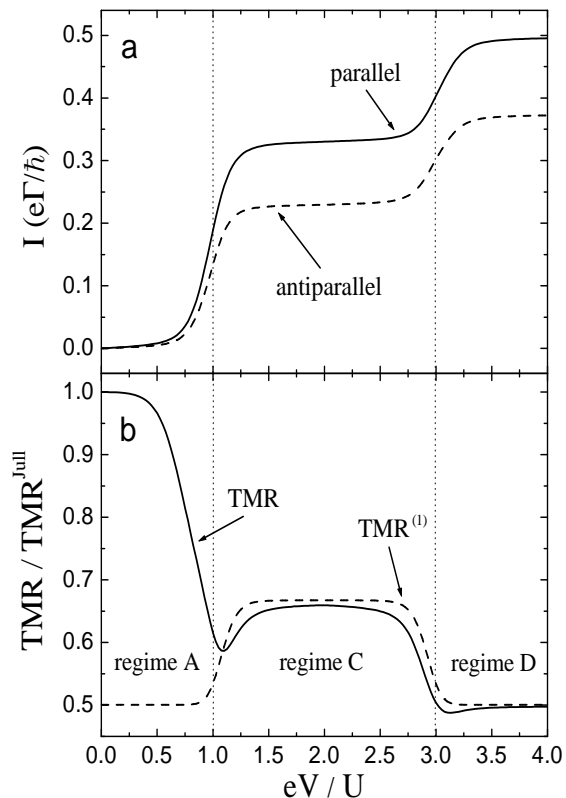


FIG. 11: The total current (a) in the parallel (solid line) and antiparallel (dashed line) magnetic configurations as a function of the bias voltage. Part (b) shows the first-order contribution to TMR (dashed line) and the total TMR (solid line). The parameters are: $k_B T = 1.5\Gamma$, $\varepsilon = 20\Gamma$, $U = 40\Gamma$, and $p = 0.5$. The figure was generated using the perturbation expansion in the presence of sequential tunneling.

nounce zero-bias anomaly of the differential conductance as a function of the bias voltage in the antiparallel configuration, as we have discussed in detail in Ref. 31. For completeness we repeat here some important facts and discuss their implications on the TMR. Deep in the Coulomb blockade regime such that the sequential tunneling contributions can be completely ignored, we can use the perturbation scheme for the Coulomb blockade valley. In Fig. 10a we show the differential conductance for both the parallel and antiparallel configurations for different values of the temperature. For the parallel alignment, the conductance shows the typical cotunneling behavior, namely a smooth parabolic dependence on the bias voltage. This contrasts with the antiparallel configuration, for which the differential conductance has a pronounced zero-bias peak sitting at the bottom of a parabola. The width of the zero-bias peak is governed by temperature, indicating different spin-accumulation behavior for $|eV| \ll k_B T$ and $|eV| \gg k_B T$.

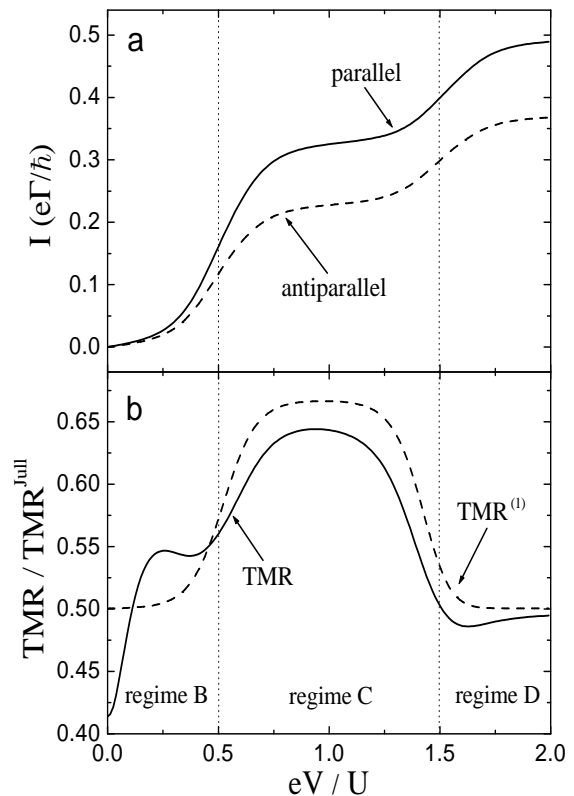


FIG. 12: The total current (a) in the parallel (solid line) and antiparallel (dashed line) magnetic configuration as a function of the bias voltage. Part (b) shows the first-order contribution to the TMR (dashed line) and the total TMR (solid line). The parameters are: $k_B T = 1.5\Gamma$, $\varepsilon = -10\Gamma$, $U = 40\Gamma$, and $p = 0.5$. The figure was generated using the perturbation expansion in the presence of sequential tunneling.

3. Regime C

In Fig. 11 we show the current for the parallel and antiparallel configuration and the resulting TMR for the situation when the dot level lies above the Fermi energy of the leads. The first-order TMR is also shown for comparison. In this case, one crosses over from regime A via C to D as the bias voltage is increased. At low voltage, regime A, current is carried by non-spin-flip cotunneling, with the TMR given by Julliere's value. Once the threshold to regime C is reached, sequential tunneling plays the dominant role. Second-order corrections to the current give rise to a slightly reduced TMR as compared to the sequential tunneling value. To find an approximate analytic expression for this case, we consider the case of zero temperature, expand the TMR up to first order in Γ and assume $|\varepsilon|/U \ll 1$ to get

$$\text{TMR}^C = \frac{p^2}{1-p^2} \left[\frac{4}{3} - \frac{(27+34p^2+3p^4)\Gamma}{18\pi(1-p^2)\varepsilon} \right]. \quad (28)$$

At the intersection of regimes A and C the TMR develops a local minimum. This is a consequence of

the fact that when approaching the intersection from regime C the sequential-tunneling-dominated TMR decreases while beyond, in regime A, the TMR has to rise again to reach Julliere's value [35].

In Fig. 12 we show the current as well as the first-order and total TMR as a function of bias voltage for $\varepsilon = -10\Gamma$. In this case, there is a crossover from regime B via C to D. Again, there is a local minimum of the TMR at the threshold to sequential tunneling due to the same reason as above.

4. Regime D

In regime D all the four dot states, i.e., $\chi = 0, \uparrow, \downarrow, d$ take part in transport. This situation is illustrated in Fig. 11 for $eV > 2(\varepsilon + U)$. In this regime, transport is dominated by the first-order processes and the influence of second-order processes is negligible. Consequently, the value of total TMR in regime D is well described by Eq. (21), as can be seen in Figs. 9b and 11b.

E. Signature of exchange field

It has been predicted [19, 36] by some of us that the coupling of the dot levels to spin-polarized leads gives rise to an effective exchange field seen by the quantum dot electrons (an overview about the various effects of this exchange field is given in Ref. 37). This exchange field is a consequence of both the Coulomb interaction on the dot and the spin polarization in the leads. The contribution coming from one lead is proportional to the degree of spin polarization p and the tunnel-coupling strength Γ . Its direction is collinear with the leads' magnetization and its magnitude and even the sign is a function of the level position relative to the Fermi level. The total exchange field experienced by the dot electrons is the (vector) sum of the two leads' contribution. This exchange field gives rise to nontrivial transport behavior associated with a precession of the accumulated spin in the sequential-tunneling regime for noncollinearly magnetized leads [19, 20, 22] and leads to a splitting of the Kondo resonance in the strong-coupling limit [36, 38], as experimentally observed recently [14]. By applying our diagrammatic technique, the exchange field is automatically included.

As we argue in the following, the exchange field will, under certain circumstances, also show up in the parameter regime studied in this paper, namely as an *equilibrium* spin polarization of the dot. This is distinctively different from the *nonequilibrium* spin accumulation discussed in the previous sections. The latter is a nonequilibrium effect that changes sign with bias reversal and, in particular, vanishes for zero bias voltage. In contrast, a finite spin polarization at equilibrium can only occur when the dot level is spin split by either an external magnetic field

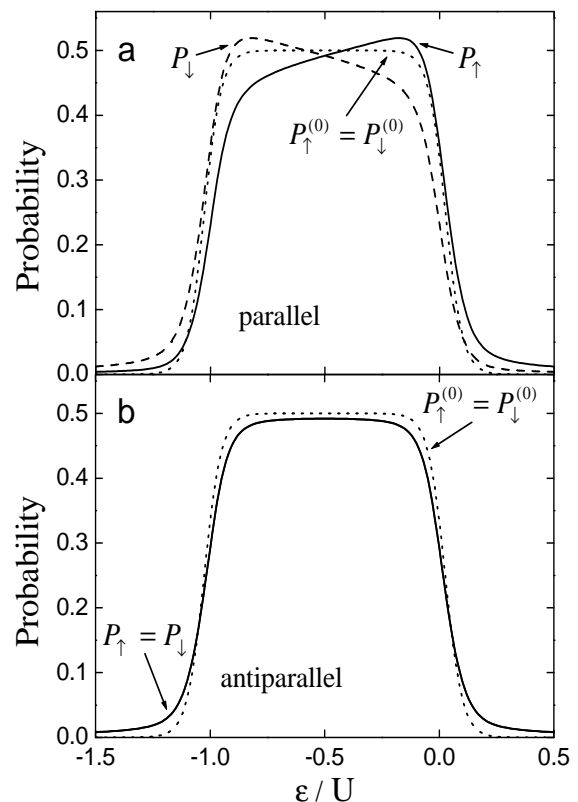


FIG. 13: The occupation probabilities of the spin-up and spin-down dot levels as a function of the level position in the parallel (a) and antiparallel (b) configuration. The zeroth-order occupation probabilities for the spin-up and spin-down levels are equal in both magnetic configurations, and are represented by the dotted lines. The total occupation probability of the spin-up (spin-down) level is presented by the solid (dashed) line. In the antiparallel configuration, the dashed and solid lines coincide. The parameters are: $k_B T = 1.5\Gamma$, $U = 40\Gamma$, and $p = 0.5$. The figure was generated using the scheme for the perturbation expansion in the presence of sequential tunneling.

or by the intrinsic exchange field that we want to address now.

In the antiparallel configuration, and for symmetric coupling to and equal spin polarization of the leads, the exchange-field contributions from the two leads exactly cancel out each other since they are of equal magnitude but pointing in opposite directions. This is different for the parallel configuration, for which the contributions from the two leads add up to some finite value.

To lowest (zeroth) order in the tunnel coupling strengths Γ , the equilibrium probabilities for occupation with spin $\sigma = \uparrow, \downarrow$ are determined by the Boltzmann factors $P_\uparrow^{(0)} = P_\downarrow^{(0)} = \exp(-\beta\varepsilon)/Z$, where Z denotes the partition function. Since the exchange field is proportional to Γ , it does not affect the zeroth-order occupation probabilities, i.e., the sequential-tunneling approximation is not able to describe the exchange-field induced spin polarization. This is shown in Fig. 13, where

the equilibrium probabilities calculated to zeroth- and zeroth- plus first-order in the dot-lead coupling are presented. A finite spin polarization for the parallel configuration is only generated by the first-order corrections $P_{\uparrow}^{(1)} \neq P_{\downarrow}^{(1)}$, that we obtain by solving the master equation given by Eq. (13). The ε -dependence of the spin polarization seen in Fig. 13 reflects the ε -dependence of the exchange field. The exchange field for a particle-hole symmetric band vanishes in the middle of the Coulomb blockade valley, $\varepsilon = -U/2$, and has different sign on either side. As a consequence the dot polarization changes sign as well.

Since in regime B $\Sigma_{\chi\sigma}^{I(1)}$ are exponentially suppressed, the exchange splitting and probabilities $P_{\sigma}^{(1)}$ do not affect the second-order transport. These probabilities affect only higher-order transport contributions, which at low temperature $T \lesssim T_K$ lead to the Kondo effect [14, 36, 38].

V. SUMMARY

We have discussed electronic transport through quantum dots coupled to ferromagnetic leads. Based on a formalism that allows for a systematic perturbation expansion in the tunnel coupling strength, we analyzed the TMR through a single-level quantum dot for the linear- and nonlinear-response regime, at or off resonance, with an even or odd dot electron number. We found different TMR values for different transport regimes. In addition to the full numerical results we provided approximate analytic expressions for various limiting cases. The most important findings are:

- (i) Except for the Coulomb-blockade valley with an even dot-electron number and the nonlinear-response regime of the Coulomb-blockade valley with an odd dot-electron number, the TMR is below that of a single magnetic tunnel junction.
- (ii) There is an even-odd asymmetry between the Coulomb-blockade valleys with an even or odd number of electrons, that is related to the absence or presence of spin-flip cotunneling, respectively.
- (iii) In the Coulomb-blockade valley with an odd number of electrons, the TMR values for the linear and nonlinear response regimes differ strongly from each other, associated with different spin-relaxation processes that affect the spin accumulation.
- (iv) The linear-response TMR in the Coulomb-blockade valley with an odd number of electrons is a function of gate voltage, which reflects the relative importance of spin-flip and non-spin-flip cotunneling.
- (v) The TMR at the onset of sequential tunneling displays a local minimum, which is a consequence of interpolating the TMR behavior away from resonance.

Acknowledgments

We thank Matthias Braun, Matthias Hettler, Ken Imura, Sadamichi Maekawa, Axel Thielmann for helpful discussions. The work was supported by the Deutsche Forschungsgemeinschaft through SFB491 and GRK726, the Polish State Committee for Scientific Research through the projects PBZ/KBN/044/P03/2001 and 2 P03B 116 25, "Spintronics" RT Network of the EC Grant No. RTN2-2001-00440, and the Center of Excellence for Magnetic and Molecular Materials for Future Electronics within the EC Contract G5MA-CT-2002-04049.

APPENDIX A: DIAGRAMMATIC TECHNIQUE

In this Appendix we present general rules in energy space for calculating contributions of various diagrams. We also present an exemplary calculation of one of the second-order self-energies. Afterwards, we show how to determine self-energies contributing to electric current.

1. Rules in energy space

Contribution of a particular diagram to the self-energy $\Sigma_{\chi'\chi}$ can be found following the general rules in the energy space:

1. Draw all topologically different diagrams with fixed time ordering and position of vertices. Connect the vertices by tunneling lines. Assign the energies of respective quantum dot states to the forward and backward propagators. To each tunneling line assign a frequency ω , the spin of tunneling electron and label of the junction.
2. Tunneling lines acquire arrows indicating whether an electron leaves or enters the dot. For tunneling lines going forward with respect to the Keldysh contour assign a factor $\gamma_r^{-\sigma}(\omega)$, whereas for tunneling lines going backward assign $\gamma_r^{+\sigma}(\omega)$.
3. For each time interval on the real axis limited by two adjacent vertices draw a vertical line inside the interval and assign a resolvent $1/(\Delta E + i0^+)$, with ΔE being the difference of all energies crossing the vertical line from right minus all energies crossing the vertical line from left.
4. Each diagram gets a prefactor $(-1)^{b+c}$, with b being the number of vertices lying on the backward propagator and c denoting the number of crossings of the tunneling lines.
5. Each internal vertex represents a matrix element $\langle \chi | A | \chi' \rangle$, with A being a dot operator, $A = d_{\sigma}^{\dagger}, d_{\sigma}$. Consequently, a minus sign may appear due to these matrix elements. This is because |d) =

$d_{\sigma}^{\dagger}|\bar{\sigma}\rangle = -d_{\sigma}^{\dagger}|\sigma\rangle$ (depending on the definition of state $|d\rangle$), where $\sigma = \uparrow$ or $\sigma = \downarrow$. To account for this factor, multiply each diagram by $(-1)^m$, where m is the number of vertices connecting the spin- σ state with doubly occupied state.

6. Integrate over all frequencies and sum up over the reservoirs.

The parameters $\gamma_r^{\pm\sigma}(\omega)$ are defined as

$$\gamma_r^{+\sigma}(\omega) = \frac{\Gamma_r^{\sigma}}{2\pi} f(\omega - \mu_r), \quad (\text{A1})$$

$$\gamma_r^{-\sigma}(\omega) = \frac{\Gamma_r^{\sigma}}{2\pi} [1 - f(\omega - \mu_r)], \quad (\text{A2})$$

with $f(x)$ being the Fermi-Dirac distribution function, $f(x) = 1/[\exp(x/k_B T) + 1]$, and μ_r representing the electrochemical potential of lead r .

2. Calculation of $\Sigma_{\bar{\sigma}\sigma}^{(2)}$

In order to find the zeroth-order and first-order probabilities, one needs to determine all the self-energies of first and second order in Γ . Below, we present an exemplary calculation of one of the second-order self-energies, $\Sigma_{\bar{\sigma}\sigma}^{(2)}$. The equation for $\Sigma_{\bar{\sigma}\sigma}^{(2)}$ can be graphically presented as

$$\Sigma_{\bar{\sigma}\sigma}^{(2)} = \begin{array}{cccccc} \sigma \begin{array}{c} d \\ \bar{\sigma} \\ \sigma \end{array} \begin{array}{c} \bar{\sigma} \\ \sigma \end{array} \bar{\sigma} & \sigma \begin{array}{c} \sigma \\ \sigma \end{array} \begin{array}{c} 0 \\ \bar{\sigma} \end{array} \bar{\sigma} & \sigma \begin{array}{c} \sigma \\ \sigma \end{array} \begin{array}{c} d \\ 0 \end{array} \bar{\sigma} & \sigma \begin{array}{c} d \\ \bar{\sigma} \\ \sigma \end{array} \begin{array}{c} \bar{\sigma} \\ \sigma \end{array} \bar{\sigma} & \sigma \begin{array}{c} d \\ \bar{\sigma} \\ \sigma \end{array} \begin{array}{c} \bar{\sigma} \\ \sigma \end{array} \bar{\sigma} & \sigma \begin{array}{c} d \\ \bar{\sigma} \\ \sigma \end{array} \begin{array}{c} \bar{\sigma} \\ \sigma \end{array} \bar{\sigma} \\ \sigma \begin{array}{c} \sigma \\ \sigma \end{array} \begin{array}{c} d \\ \bar{\sigma} \\ \sigma \end{array} \bar{\sigma} & \sigma \begin{array}{c} \sigma \\ \sigma \end{array} \begin{array}{c} \sigma \\ \bar{\sigma} \\ \sigma \end{array} \bar{\sigma} & \sigma \begin{array}{c} d \\ \bar{\sigma} \\ \sigma \end{array} \begin{array}{c} \bar{\sigma} \\ \sigma \end{array} \bar{\sigma} & \sigma \begin{array}{c} d \\ \bar{\sigma} \\ \sigma \end{array} \begin{array}{c} \bar{\sigma} \\ \sigma \end{array} \bar{\sigma} & \sigma \begin{array}{c} \sigma \\ \sigma \end{array} \begin{array}{c} d \\ \bar{\sigma} \\ \sigma \end{array} \bar{\sigma} & \sigma \begin{array}{c} 0 \\ \bar{\sigma} \\ \sigma \end{array} \begin{array}{c} \bar{\sigma} \\ \sigma \end{array} \bar{\sigma} \\ \sigma \begin{array}{c} \sigma \\ \sigma \end{array} \begin{array}{c} 0 \\ \bar{\sigma} \\ \sigma \end{array} \bar{\sigma} & \sigma \begin{array}{c} \sigma \\ \sigma \end{array} \begin{array}{c} \sigma \\ \bar{\sigma} \\ \sigma \end{array} \bar{\sigma} & \sigma \begin{array}{c} d \\ \bar{\sigma} \\ \sigma \end{array} \begin{array}{c} \bar{\sigma} \\ \sigma \end{array} \bar{\sigma} & \sigma \begin{array}{c} 0 \\ \bar{\sigma} \\ \sigma \end{array} \begin{array}{c} \bar{\sigma} \\ \sigma \end{array} \bar{\sigma} & \sigma \begin{array}{c} \sigma \\ \sigma \end{array} \begin{array}{c} \sigma \\ \bar{\sigma} \\ \sigma \end{array} \bar{\sigma} & \sigma \begin{array}{c} \sigma \\ \sigma \end{array} \begin{array}{c} 0 \\ \bar{\sigma} \\ \sigma \end{array} \bar{\sigma} \\ \sigma \begin{array}{c} \sigma \\ \sigma \end{array} \begin{array}{c} d \\ \bar{\sigma} \\ \sigma \end{array} \bar{\sigma} & \sigma \begin{array}{c} \sigma \\ \sigma \end{array} \begin{array}{c} 0 \\ \bar{\sigma} \\ \sigma \end{array} \bar{\sigma} & \sigma \begin{array}{c} d \\ \bar{\sigma} \\ \sigma \end{array} \begin{array}{c} \bar{\sigma} \\ \sigma \end{array} \bar{\sigma} & \sigma \begin{array}{c} 0 \\ \bar{\sigma} \\ \sigma \end{array} \begin{array}{c} \bar{\sigma} \\ \sigma \end{array} \bar{\sigma} & \sigma \begin{array}{c} \sigma \\ \sigma \end{array} \begin{array}{c} \sigma \\ \bar{\sigma} \\ \sigma \end{array} \bar{\sigma} & \sigma \begin{array}{c} \sigma \\ \sigma \end{array} \begin{array}{c} 0 \\ \bar{\sigma} \\ \sigma \end{array} \bar{\sigma} \end{array} \quad (\text{A3})$$

To calculate the self-energy, it is necessary to evaluate each contributing diagram. As an example, we present calculation of the third diagram of Eq. (A3). Follow-

ing the general rules described above, the corresponding contribution, Λ_3 , is given by

$$\Lambda_3 = (-1)^{2+1}(-1)^1 \sum_{r_1, r_2} \iint d\omega_1 d\omega_2 \gamma_{r_1}^{-\sigma}(\omega_1) \gamma_{r_2}^{+\bar{\sigma}}(\omega_2) \frac{1}{\omega_1 - \varepsilon_{\sigma} + i0^+} \frac{1}{\omega_1 + \omega_2 - \varepsilon_{\sigma} - \varepsilon_{\bar{\sigma}} - U + i0^+} \frac{1}{\omega_2 - \varepsilon_{\bar{\sigma}} + i0^+} \quad (\text{A4})$$

The first (second) factor on the right-hand side follows from the rule 4 (5). There are also three resolvents according to the rule (3). Among the various diagrams contributing to $\Sigma_{\bar{\sigma}\sigma}^{(2)}$, there is a diagram (eleventh in Eq. A3) whose contribution is equal to minus complex conjugate of the contribution due to the third diagram, $\Lambda_{11} = -\text{Re}(\Lambda_3) + i\text{Im}(\Lambda_3)$. This can be shown by interchanging the backward and forward propagators and changing the direction of the tunneling lines. As a consequence, the real parts of these diagrams cancel, whereas the imaginary parts add to each other. Thus, it is nec-

essary to determine only the imaginary part of one of those two diagrams, $\Lambda_3 + \Lambda_{11} = 2i\text{Im}(\Lambda_3)$. After contour integration, the imaginary part of Λ_3 is given by

$$\text{Im}(\Lambda_3) = \frac{\pi}{U} \sum_{r_1, r_2} \left[\gamma_{r_1}^{-\sigma}(\varepsilon_{\sigma}) A_{1r_2}^{+\bar{\sigma}}(\varepsilon_{\bar{\sigma}}) + \gamma_{r_2}^{+\bar{\sigma}}(\varepsilon_{\bar{\sigma}}) A_{1r_1}^{-\sigma}(\varepsilon_{\sigma}) - \frac{\Gamma_{r_1}^{\sigma}}{2\pi} f_{\text{B}}(\mu_{r_1} + \mu_{r_2} - \varepsilon_{\sigma} - \varepsilon_{\bar{\sigma}} - U) X_{1r_2}^{+\bar{\sigma}}(2\mu_{r_2} - \varepsilon_{\bar{\sigma}} - U) - \frac{\Gamma_{r_2}^{\bar{\sigma}}}{2\pi} f_{\text{B}}(\varepsilon_{\sigma} + \varepsilon_{\bar{\sigma}} + U - \mu_{r_1} - \mu_{r_2}) X_{1r_1}^{+\sigma}(\varepsilon_{\sigma}) \right], \quad (\text{A5})$$

with $f_B(x)$ being the Bose-Einstein distribution function $f_B(x) = 1/[\exp(x/k_B T) - 1]$. The corresponding coefficients $A_{\alpha r}^{\pm\sigma}(\varepsilon_\sigma)$ are defined as, $A_{\alpha r}^{\pm\sigma}(\varepsilon_\sigma) = X_{\alpha r}^{\pm\sigma}(\varepsilon_\sigma) - X_{\alpha r}^{\pm\sigma}(\varepsilon_\sigma + U)$, with $X_{\alpha r}^{\pm\sigma}(\varepsilon_\sigma) = \pm\Gamma_r^\sigma/(2\pi)B_\alpha(\varepsilon_\sigma - \mu_r)$ and $B_\alpha(x)$ given by

$$B_{\alpha+1}(x) = \frac{d^{(\alpha)}}{dx^{(\alpha)}} \operatorname{Re} \left[\Psi \left(\frac{1}{2} + i \frac{x}{2\pi k_B T} \right) - \ln \left(\frac{W}{2\pi k_B T} \right) \right],$$

where $\Psi(z)$ is the digamma function, and we have used the Lorentzian cutoff function of the form $\rho_\nu(\omega) =$

$W^2/[(\omega - \mu_\nu)^2 + W^2]$, with W being the cutoff parameter. As contribution from a single diagram may depend on W , the final result does not. In the calculations the cutoff parameter was taken to be equal to 100Γ .

In a similar way, one can calculate contributions of all diagrams, which give

$$\begin{aligned} \Sigma_{\bar{\sigma}\sigma}^{(2)} = & -2\pi i \sum_{r_1, r_2} \left\{ \gamma_{r_1}^{-\sigma}(\varepsilon_\sigma) X_{2r_2}^{+\bar{\sigma}}(\varepsilon_{\bar{\sigma}}) + \gamma_{r_1}^{+\bar{\sigma}}(\varepsilon_{\bar{\sigma}}) X_{2r_2}^{-\sigma}(\varepsilon_\sigma) \right. \\ & + \gamma_{r_1}^{-\sigma}(\varepsilon_\sigma + U) X_{2r_2}^{+\bar{\sigma}}(\varepsilon_{\bar{\sigma}} + U) + \gamma_{r_1}^{+\bar{\sigma}}(\varepsilon_{\bar{\sigma}} + U) X_{2r_2}^{-\sigma}(\varepsilon_\sigma + U) \\ & - f_B(\mu_{r_1} - \mu_{r_2} + \varepsilon_{\bar{\sigma}} - \varepsilon_\sigma) \left\{ \frac{\Gamma_{r_2}^{\bar{\sigma}}}{2\pi} \left[X_{2r_1}^{+\sigma}(\varepsilon_\sigma) + X_{2r_1}^{+\sigma}(\varepsilon_\sigma + U) + \frac{2}{U} A_{r_1}^{+\sigma}(\varepsilon_\sigma) \right] \right. \\ & \left. \left. - \frac{\Gamma_{r_1}^{\sigma}}{2\pi} \left[X_{2r_2}^{+\bar{\sigma}}(\varepsilon_{\bar{\sigma}}) + X_{2r_2}^{+\bar{\sigma}}(\varepsilon_{\bar{\sigma}} + U) + \frac{2}{U} A_{r_2}^{+\bar{\sigma}}(\varepsilon_{\bar{\sigma}}) \right] \right\} \right\} \end{aligned} \quad (\text{A6})$$

3. Diagrams contributing to the current

To find current flowing through the system, one has to determine the self-energies Σ^I , see Eq. (10) or (11). This can be done by realizing that each term of the expansion of the current operator \hat{I} is equal to the corresponding expansion term of the reduced density matrix multiplied by a factor of e/\hbar . The only difference is that now for each external vertex lying on the upper (lower) branch of the Keldysh contour, corresponding to tunneling of an electron into the left (right) or out of the right (left) lead, we have a multiplicative factor $+1/2$, whereas for each external vertex on the upper (lower) branch of the

contour, describing tunneling of an electron into the right (left) or out of the left (right) lead, there is a factor of $-1/2$.

We have determined all the first-order and second-order self-energies contributing to electrical current, $\Sigma^{I(1)}$ and $\Sigma^{I(2)}$, and found that from the first-order self-energies only $\Sigma_{0\sigma}^{I(1)}$, $\Sigma_{\sigma 0}^{I(1)}$, $\Sigma_{\sigma d}^{I(1)}$, $\Sigma_{d\sigma}^{I(1)}$ give nonzero contributions. In the case of the second-order self-energies we found $\Sigma_{\chi\chi}^{I(2)} = 0$, with $\chi = 0, \uparrow, \downarrow, d$. This is however only the case for the current operator defined as $\hat{I} = (\hat{I}_R - \hat{I}_L)/2$, where \hat{I}_r is the current operator for electrons tunneling to the lead r .

-
- [1] S. A. Wolf, D. D. Awschalom, R. A. Buhrman, J. M. Daughton, S. von Molnar, M. L. Roukes, A. Y. Chtchelka, and D. M. Treger, *Science* **294**, 1488 (2001).
 - [2] J. F. Gregg, I. Petej, E. Jouguelet, and C. Dennis, *J. Phys. D: Appl. Phys.* **35**, R121 (2002).
 - [3] *Semiconductor Spintronics and Quantum Computation*, ed. by D.D. Awschalom, D. Loss, and N. Samarth (Springer, Berlin 2002).
 - [4] S. Maekawa and T. Shinjo, *Spin Dependent Transport in Magnetic Nanostructures* (Taylor & Francis 2002).
 - [5] D.V. Averin, K.K. Likharev, in *Mesoscopic Phenomenon in Solids*, ed. by B.L. Altshuler, P.A. Lee, R.A. Webb (Amsterdam: North-Holland 1991).
 - [6] *Single Charge Tunneling: Coulomb Blockade Phenomena in Nanostructures*, NATO ASI Series B: Physics 294, ed.

- by H. Grabert, M.H. Devoret (Plenum Press, New York 1992).
- [7] *Mesoscopic Electron Transport*, ed. by L.L. Sohn, L.P. Kouwenhoven, G. Schön (Kluwer, Dordrecht 1997).
- [8] J. Barnaś and A. Fert, *Phys. Rev. Lett.* **80**, 1058 (1998); S. Takahashi and S. Maekawa, *Phys. Rev. Lett.* **80**, 1758 (1998).
- [9] Y. Chye, M.E. White, E. Johnston-Halperin, B.D. Gerardot, D.D. Awschalom, and P.M. Petroff, *Phys. Rev. B* **66**, 201301(R) (2002).
- [10] M.M. Deshmukh and D.C. Ralph, *Phys. Rev. Lett.* **89**, 266803 (2002).
- [11] K. Tsukagoshi, B.W. Alphenaar, and H. Ago, *Nature* **401**, 572 (1999).
- [12] B. Zhao, I. Mönch, H. Vinzelberg, T. Mühl, and

- C.M. Schneider, Appl. Phys. Lett. **80**, 3144 (2002); J. Appl. Phys. **91**, 7026 (2002).
- [13] J. Nygard, W.F. Koehl, N. Mason, L. DiCarlo, and C.M. Marcus, cond-mat/0410467.
- [14] A. N. Pasupathy, R. C. Bialczak, J. Martinek, J. E. Grose, L. A. K. Donev, P. L. McEuen, and D. C. Ralph, Science **306**, 86 (2004).
- [15] M. Julliere, Phys. Lett. A **54**, 225 (1975).
- [16] B. R. Bulka, Phys. Rev. B **62**, 1186 (2000).
- [17] W. Rudziński and J. Barnaś, Phys. Rev. B **64**, 085318 (2001).
- [18] A. Cottet, W. Belzig, and C. Bruder, Phys. Rev. Lett. **92**, 206801 (2004).
- [19] J. König and J. Martinek, Phys. Rev. Lett. **90**, 166602 (2003).
- [20] M. Braun, J. König, J. Martinek, Phys. Rev. B **70**, 195345 (2004).
- [21] W. Rudziński, J. Barnaś, R. Świrkowicz, and M. Wilczyński, cond-mat/0409386.
- [22] S. Braig and P. W. Brouwer, cond-mat/0412592.
- [23] D. V. Averin and A. A. Odintsov, Phys. Lett. A **140**, 251 (1989).
- [24] D. V. Averin and Yu. V. Nazarov, Phys. Rev. Lett. **65**, 2446 (1990).
- [25] K. Kang and B. I. Min, Phys. Rev. B **55**, 15412 (1997).
- [26] S. De Franceschi, S. Sasaki, J. M. Elzerman, W. G. van der Wiel, S. Tarucha, and L. P. Kouwenhoven, Phys. Rev. Lett. **86**, 878 (2001).
- [27] A. Kogan, S. Amasha, D. Goldhaber-Gordon, G. Granger, M.A. Kastner, and H. Shtrikman, Phys. Rev. Lett. **93**, 166602 (2004).
- [28] D. M. Zumbühl, C. M. Marcus, M. P. Hanson, and A. C. Gossard, Phys. Rev. Lett. **93**, 256801 (2004).
- [29] M. Ciorga, M. Pioro-Ladrère, P. Zawadzki, J. Lapointe, Z. Wasilewski, and A. S. Sachrajda, cond-mat/0407071.
- [30] J. König, *Quantum Fluctuations in the Single-Electron Transistor*, (Shaker, Aachen, 1999).
- [31] I. Weymann, J. Barnaś, J. König, J. Martinek, and G. Schön, cond-mat/0412434.
- [32] H. Schoeller and G. Schön, Phys. Rev. B **50**, 18436 (1994); J. König, J. Schmid, H. Schoeller, and G. Schön, Phys. Rev. B **54**, 16820 (1996).
- [33] A. Thielmann, M. H. Hettler, J. König, and G. Schön, Phys. Rev. B **68**, 165341 (2003).
- [34] H. Imamura, S. Takahashi, and S. Maekawa, Phys. Rev. B **59**, 6017 (1999).
- [35] R. Świrkowicz, J. Barnaś, and M. Wilczyński, J. Phys.: Condens. Matter **14**, 2011 (2002).
- [36] J. Martinek, Y. Utsumi, H. Imamura, J. Barnaś, S. Maekawa, J. König, and G. Schön, Phys. Rev. Lett. **91**, 127203 (2003).
- [37] J. König, J. Martinek, J. Barnas, and G. Schön, in *CFN Lectures on Functional Nanostructures*, Eds. K. Busch et al., Lecture Notes in Physics **658**, Springer, 145 (2005); cond-mat/0404509.
- [38] J. Martinek, M. Sindel, L. Borda, J. Barna, J. König, G. Schön, and J. von Delft, Phys. Rev. Lett. **91**, 247202 (2003); M.S. Choi, D. Sanchez, and R. Lopez, Phys. Rev. Lett. **92**, 056601 (2004).